Hindawi Publishing Corporation
International Journal of Antennas and Propagation
Volume 2015, Article ID 147368, 12 pages
http://dx.doi.org/10.1155/2015/147368

Research Article

Target Detection in Low Grazing Angle with Adaptive OFDM Radar

Yang Xia, Zhiyong Song, Zaiqi Lu, Hao Wu, and Qiang Fu

ATR Key Laboratory, National University of Defense Technology, Changsha, Hunan 410073, China

Correspondence should be addressed to Yang Xia; xiayang2020@126.com

Received 10 June 2015; Revised 31 August 2015; Accepted 7 October 2015

Academic Editor: Kyeong Jin Kim

Multipath effect is the main factor of deteriorating target detection performance in low grazing angle scenario, which results from reflections on the ground/sea surface. Amplitudes of the received signals fluctuate acutely due to the random phase variations of reflected signals along different paths; thereby the performances of target detection and tracking are heavily influenced. This paper deals with target detection in low grazing angle scenario with orthogonal frequency division multiplexing (OFDM) radar. Realistic physical and statistical effects are incorporated into the multipath propagation model. By taking advantage of multipath propagation that provides spatial diversity of radar system and frequency diversity of OFDM waveform, we derive a detection method based on generalized likelihood ratio test (GLRT). Then, we propose an algorithm to optimally design the transmitted subcarrier weights to improve the detection performance. Simulation results show that the detection performance can be improved due to the multipath effect and adaptive OFDM waveform design.

1. Introduction

Target detection and tracking in low grazing angle scenario is one of the most challenging problems in radar community [1]. Multipath effect is the main problem when detecting targets in low grazing angle scenario. Amplitudes of received signals fluctuate acutely due to random phase (which is decided by differential path length, wavelength, and characteristics of reflected surface [2]) variations between different paths; thereby the detection performance is deteriorated. Currently, researches on multipath effect are mainly focused on two aspects: suppressing multipath and utilizing it [3]. From another point of view, multipath echoes also contain target energy and the detection performance may be enhanced if the energy from multipath reflections is accumulated.

Orthogonal frequency division multiplexing (OFDM) was originally proposed as a digital modulation technique in communication fields. Later on, it was introduced into radar community [4]. As a new broadband radar signal, OFDM signal advances in high spectral efficiency, low probability of intercept, and frequency diversity [5–7]. An adaptive technique to design the spectrum of OFDM was proposed in [8] by incorporating the scattering coefficients of the target at multiple frequencies and the results showed that the wideband ambiguity function (WAF) was improved due to the adaptive waveform design. Similar OFDM waveform design method can also be found in [9, 10].

Focusing on the issue of target detection in urban environment, an optimized detection algorithm based on OFDM radar was proposed in [11, 12]. The results demonstrated that the detection performance was improved by utilizing multipath reflections. However, the proposed signal model was idealistic and only considered specular reflections. The problem of target detection in multipath scenarios was reformulated as sparse spectrum estimation, where the spectral parameters of OFDM radar signal are optimized to improve the detection performance using multiobjective optimization (MOO) technique [13, 14]. The performances of generalized likelihood ratio test (GLRT) detector with OFDM radar in non-Gaussian clutter (log-normal, Weibull, and K-compound) were investigated in [15], where target fluctuations were also taken into consideration. Consequently,

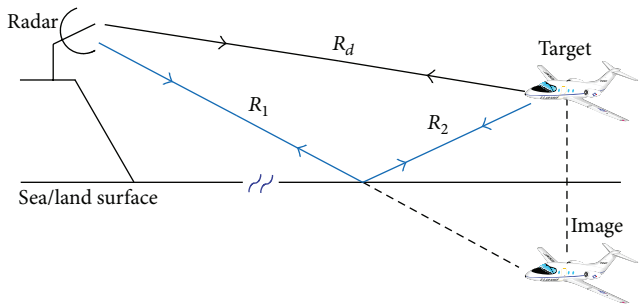

Figure 1: Representative scenario of multipath propagation in low grazing angle.

detection performance may be enhanced with OFDM radar in low grazing angle scenario by utilizing multipath reflections.

When detecting target in low grazing angle scenario, radar measurements are affected by many factors, such as ever-changing meteorological conditions in the troposphere, Earth's curvature, and roughness of ground/sea surface [16]. All these factors will affect the detection performance and, therefore, these factors should be taken into consideration to make the signal model more realistic.

This paper deals with target detection in low grazing angle scenario with OFDM radar. To make the propagation model more accurate, refraction of the lower atmosphere and the Earth's curvature are taken into consideration, and the multipath propagation model is modified accordingly. Based on the characteristics of OFDM radar, we derive a GLRT detector in Gaussian clutter environment. Then a waveform design method which optimizes the transmitted subcarrier weights is proposed to improve the detection performance. Finally, the performance of the proposed detector is analyzed and discussed via simulation experiments.

2. Modified Multipath Propagation Model

Multipath effect is one of the main problems when detecting and tracking target in low grazing angle scenario. The echo signals received by radar receiver not only include direct signals but also include indirect signals. Thus, the received signals are the sum of reflected signals along different paths and the amplitudes fluctuate acutely due to the random phase variations, which deteriorates the performances of target detection and tracking. Generally speaking, signals reflected more than twice will be attenuated heavily, which can always be neglected.

The representative scenario of multipath propagation in low grazing angle is shown in Figure 1. Target locates at a distance R_d from the radar. The source is assumed to be a narrowband signal, which can be represented as [16]

$$x(t) = ae^{j(\omega t+\xi)}, \tag{1}$$

where a, ω, and ξ denote the amplitude, angular frequency, and initial phase, respectively. In the presence of multipath, the received signals consist of two components, namely, the direct and indirect signals. Direct signal is given by

$$x_d(t) = x(t)\, e^{-j(2\pi/\lambda)(2R_d)} \tag{2}$$

and the indirect signal is

$$x_i(t) = x(t)\, \rho e^{j\varphi} e^{-j(2\pi/\lambda)R_i}. \tag{3}$$

In (3), $\rho e^{j\varphi}$ is the complex reflection coefficient and R_i is the total length of indirect path. For first-order reflected signals, $R_i = R_1 + R_2 + R_d$ and, for second-order reflected signals, $R_i = 2(R_1 + R_2)$. Received signal can be represented as

$$\begin{aligned} x_r(t) &= x_d(t) + x_i(t) \\ &= x(t)\, e^{j(2\pi/\lambda)(2R_d)} \left(1 + \rho e^{j(\varphi+(2\pi/\lambda)\Delta R)}\right), \end{aligned} \tag{4}$$

where $\Delta R = R_i - 2R_d$. In (4), the amplitudes of received signals are dependent on the factor $\rho e^{j(\varphi+(2\pi/\lambda)\Delta R)}$, which includes the effects of complex reflection coefficient $\rho e^{j\varphi}$, wavelength λ, and path difference ΔR.

In normal atmospheric conditions, the pressure decreases exponentially with height, which causes a reduction in the refractivity with respect to height. Under this condition, a radio ray will diffract downward [17]. Furthermore, in maritime environment evaporation duct effect may be produced due to the strong humidity gradients above (within first few meters) the air-sea boundary [18], which makes a radio ray bend downward with a curvature more than the Earth's radius. The effect is dependent on a few factors such as temperature difference between the air and sea, and the wind speed [19].

In addition to the atmospheric effects, low grazing angle propagation is also affected by the fact that the Earth is curved. The curvature of the Earth decreases the path length difference between the direct and reflected waves, and it also reduces the amplitudes of the reflected waves [19]. This problem is usually dealt with by replacing the Earth with an imaginary flat Earth whose equivalent radius is

$$R_e = R_0 \left(1 + R_0 \frac{dN}{dh} 10^{-6}\right)^{-1}, \tag{5}$$

where R_0 is the radius of actual Earth and dN/dh is the refractivity gradient. For standard atmosphere, $-79 \le dN/dh \le 0$ N-units/km [19].

Considering all the factors mentioned above and based on ideal propagation model described in Figure 1, modified multipath propagation model is shown in Figure 2. The height of radar and target is h_r and h_t, respectively. The ground distance separated by radar and target is r. h_r' and h_t' are the modified heights corresponding to radar and target over flat-Earth model. r_1 is the ground distance between radar and the reflected point and ψ is the grazing angle.

In order to calculate complex reflection coefficient in (4), we have to solve the grazing angle ψ and ΔR first. These variables are all related to r_1, which can be evaluated using the following cubic equation [20]:

$$2r_1^3 - 3rr_1^2 + \left[r^2 - 2R_e\left(h_r + h_t\right)\right] r_1 + 2R_e h_r r = 0. \tag{6}$$

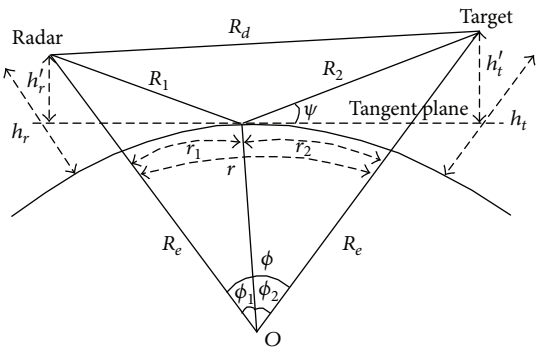

Figure 2: Modified multipath propagation model.

Then we solve h_r' and h_t' by

$$h_r' \simeq h_r - \frac{r_1^2}{2R_e},$$
$$h_t' \simeq h_t - \frac{(r-r_1)^2}{2R_e}. \tag{7}$$

Meanwhile, we can get $\phi_1 = r_1/R_e$ and $\phi_2 = (r-r_1)/R_e$. Using law of cosine yields

$$R_1 = \sqrt{R_e^2 + (R_e+h_r)^2 - 2R_e(R_e+h_r)\cos\phi_1},$$
$$R_2 = \sqrt{R_e^2 + (R_e+h_t)^2 - 2R_e(R_e+h_t)\cos\phi_2},$$
$$R_d = \sqrt{(R_e+h_r)^2 + (R_e+h_t)^2 - 2(R_e+h_r)(R_e+h_t)\cos\phi}. \tag{8}$$

Finally, the grazing angle ψ is given by

$$\psi = \frac{1}{2}\left(\pi - \arccos\left(\frac{R_1^2 + R_2^2 - R_d^2}{2R_1R_2}\right)\right). \tag{9}$$

The complex reflection coefficient can be calculated by [20]

$$\rho e^{j\varphi} = \Gamma_{(v,h)} DS, \tag{10}$$

where $\Gamma_{(v,h)}$ is vertical polarization or horizontal polarization reflection coefficient for a plane surface, D is the divergence factor due to a curved surface, and S is root-mean-squared (RMS) specular scattering coefficient which represents the roughness of surface.

$\Gamma_{(v,h)}$ is determined by frequency, complex dielectric constant, and grazing angle ψ, which can be calculated by [21]

$$\Gamma_v \simeq \frac{\sin\psi\sqrt{\varepsilon_c} - 1}{\sin\psi\sqrt{\varepsilon_c} + 1} \tag{11}$$

for vertical polarization and

$$\Gamma_h \simeq \frac{\sin\psi - \sqrt{\varepsilon_c}}{\sin\psi + \sqrt{\varepsilon_c}} \tag{12}$$

for horizontal polarization, where ε_c is complex dielectric constant which is given by $\varepsilon_c = \varepsilon/\varepsilon_0 - j60\lambda\sigma$. $\varepsilon/\varepsilon_0$ is relative dielectric constant of the reflecting medium and σ is its conductivity.

When the electromagnetic wave is incident on the surface of the Earth, due to the slight differences in each incident ray, the reflected wave is diverged and the reflected energy is defocused. When this happens, radar power density will be reduced. If the grazing angle is not large, divergence factor D can be approximated by [21]

$$D \simeq \left(1 + \frac{2r_1r_2}{R_e r\psi}\right)^{-1/2}. \tag{13}$$

Due to the reflection of rough surface, two components will be generated: a diffuse component and a coherent component with reduced magnitude. The reduction in the magnitude of the coherent component brought about by reflections from a rough surface is related to the grazing angle and the signal wavelength, which is [21]

$$S = e^{-\mu}, \tag{14}$$

where

$$\mu = \begin{cases} 2[2\pi\eta]^2 & \eta \le 0.1 \text{ rad} \\ 0.16\eta^2 + 7.42\eta + 0.0468 & \text{otherwise} \end{cases} \tag{15}$$

and η is the surface roughness factor defined as $\eta = \sigma_H\psi/\lambda$. σ_H is the RMS of reflection surface and σ_H/λ denotes the roughness of reflected surface. The larger σ_H/λ is, the more roughness the surface will be. For smooth surface, σ_H/λ is approximated to be zero.

Substituting (11)–(15) into (10), we can get the complex reflection coefficient $\rho e^{j\varphi}$. At the same time, $\rho e^{j(\varphi+(2\pi/\lambda)\Delta R)}$ can be evaluated which is the impact of multipath propagation on signal model.

3. Measurement Model of OFDM Radar

We consider a monostatic radar employing an OFDM signaling system. The transmitted signal can be described as

$$s(t) = \sum_{m=0}^{M-1} u(t - mT_r) e^{j2\pi f_0 t}, \tag{16}$$

where f_0, M, and T_r represent the carrier frequency, pulse number, and pulse repetition interval (PRI), respectively. $u(t)$ is the complex envelop of a single pulse which is given by

$$u(t) = \sum_{n=0}^{N-1} w_n \text{rect}(t, t_b) e^{j2\pi n\Delta f t}, \tag{17}$$

where

$$\text{rect}(t, t_b) = \begin{cases} 1 & 0 \le t \le t_b \\ 0 & \text{otherwise} \end{cases} \tag{18}$$

and N is the subcarrier number. $\mathbf{w} = [w_0, w_1, \ldots, w_{N-1}]^T$ represent the complex weights transmitted over different subcarriers and satisfying $\sum_{n=0}^{N-1} |w_n|^2 = 1$. For the sake of keeping orthogonality between different subcarriers, the subcarrier spacing Δf and time duration t_b of a single pulse should satisfy $\Delta f t_b = 1$. The total bandwidth is $B = N\Delta f$.

Assuming that the received signals contain P different paths and the roundtrip delay corresponding to pth path is τ_p, $p = 0, 1, \ldots, P-1$. The received signal is

$$y(t) = \sum_{p=0}^{P-1} s\left(\gamma_p\left(t - \tau_p\right)\right), \tag{19}$$

where $\gamma_p = 1 + \beta_p$ accounts for the stretching or compressing in time of the reflected signal and $\beta_p = 2\langle \mathbf{v}, \mathbf{u}_p \rangle / c$ represents the Doppler spreading factor corresponding to pth path; $\mathbf{v}$ and $\mathbf{u}_p$ are the target velocity and unit direction of arrival (DOA) vector; c is the propagation speed. Substituting (16) into (19), the received signal after demodulation is denoted by

$$\begin{aligned} y(t) &= \sum_{p=0}^{P-1} \sum_{m=0}^{M-1} u\left(\gamma_p\left(t - \tau_p\right) - mT_r\right) e^{j2\pi f_0 \beta_p (t-\tau_0)} e^{-j2\pi f_0 \tau_0} \\ &\quad + e(t). \end{aligned} \tag{20}$$

Then substituting (17) into (20), we obtain

$$\begin{aligned} y(t) = \sum_{m=0}^{M-1} \sum_{n=0}^{N-1} \sum_{p=0}^{P-1} w_n x_{np} \operatorname{rect}\left(\gamma_p\left(t - \tau_p\right) - mT_r, t_b\right) \\ \cdot e^{j2\pi n \Delta f (\gamma_p (t-\tau_p) - mT_r)} e^{j2\pi f_0 \beta_p (t-\tau_0)} e^{-j2\pi f_0 \tau_0} + e(t), \end{aligned} \tag{21}$$

where x_{np} represents the complex scattering coefficient of target corresponding to nth carrier and pth path. τ_0 is the roundtrip delay corresponding to the range cell under consideration. The relative time gaps between different paths are very small compared to the actual roundtrip delay, which means $\tau_p \approx \tau_0$ for $p = 0, 1, \ldots, P-1$. Substituting $t = \tau_0 + mT_r$ ($m = 0, 1, \ldots, M-1$) into (21), we obtain

$$y(n, m) = \sum_{p=0}^{P-1} w_n x_{np} \phi_{np}(m, v) + e(n, m), \tag{22}$$

where

$$\phi_{np}(m, v) = e^{-j2\pi f_0 \tau_0} e^{j2\pi f_n \beta_p m T_r} \tag{23}$$

and $f_n = f_0 + n\Delta f$. Equation (22) can be written into matrix form

$$\mathbf{y}(m) = \mathbf{W}\mathbf{X}\mathbf{\Phi}(m, \mathbf{v}) + \mathbf{e}(m), \tag{24}$$

where

(i) $\mathbf{y}(m) = [y(0, m), y(1, m), \ldots, y(N-1, m)]^T$ is an $N \times 1$ vector that represents output of the mth pulse,

(ii) $\mathbf{W} = \operatorname{diag}(\mathbf{w})$ is an $N \times N$ complex diagonal matrix that contains transmitted subcarrier weights,

(iii) $\mathbf{X} = \operatorname{blkdiag}(\mathbf{x}_0^T, \mathbf{x}_1^T, \ldots, \mathbf{x}_{N-1}^T)$ is an $N \times NP$ complex rectangular block-diagonal matrix; $\mathbf{x}_n = x_n \cdot \boldsymbol{\rho}$, $n = 0, 1, \ldots, N-1$, where x_n is target scattering coefficient on the nth subcarrier and $\boldsymbol{\rho} = [\rho_0, \rho_1, \ldots, \rho_{P-1}]^T$ represents complex reflection coefficients over different paths; for direct signals, $\rho_p = 1$; for first-order reflected signals, $\rho_p = \rho e^{j\varphi}$; for second-order reflected signals, $\rho_p = (\rho e^{j\varphi})^2$, where $\rho e^{j\varphi}$ is calculated by (10),

(iv) $\mathbf{\Phi}(m, \mathbf{v}) = [\phi_0(m, \mathbf{v}), \phi_1(m, \mathbf{v}), \ldots, \phi_{N-1}(m, \mathbf{v})]^T$ is an $NP \times 1$ complex vector and $\phi_n(m, \mathbf{v}) = [\phi_{n0}(m, \mathbf{v}), \phi_{n1}(m, \mathbf{v}), \ldots, \phi_{nP-1}(m, \mathbf{v})]^T$, $n = 0, 1, \ldots, N-1$,

(v) $\mathbf{e}(m) = [e_0(m), e_1(m), \ldots, e_{N-1}(m)]^T$ is an $N \times 1$ complex vector of clutter.

Then concatenating all temporal data into $N \times M$ matrix the OFDM measurement model in low grazing angle is

$$\mathbf{Y} = \mathbf{W}\mathbf{X}\mathbf{\Phi}(\mathbf{v}) + \mathbf{E}, \tag{25}$$

where

$$\mathbf{Y} = \left[\mathbf{y}(0), \mathbf{y}(1), \ldots, \mathbf{y}(M-1)\right]. \tag{26}$$

$\mathbf{\Phi}(v) = [\mathbf{\Phi}(0, v), \mathbf{\Phi}(1, v), \ldots, \mathbf{\Phi}(M-1, v)]$ is an $NP \times M$ complex matrix that contains Doppler information over M pulses.

$\mathbf{E} = [\mathbf{e}(0), \mathbf{e}(1), \ldots, \mathbf{e}(M-1)]$ is an $N \times M$ complex matrix that consists of clutter returns.

In low grazing angle scenario, the clutter is usually modeled as compound-Gaussian model which is the product of speckle and texture [22]. The speckle is fast-changing and modeled as a complex Gaussian process while the texture is slow-changing and modeled as a nonnegative process [23].

In this paper, the correlation length of the texture is assumed to be on the order of seconds and we only consider one coherent processing interval (CPI) which is assumed to be 60 ms. Due to the long correlation time of texture, it is considered to be constant within each CPI, changing according to a given probability density function (PDF) from one CPI to the next. Thus conditioned on a given value of the texture, the clutter is simplified to Gaussian distribution. However, this simplification is not justified when predicting the clutter's behavior in time intervals larger than a CPI, such as clutter cancellation and constant false alarm rate (CFAR) detection.

Thus, we assume that the clutter is temporally white and circularly zero-mean complex Gaussian process with unknown positive definite covariance $\mathbf{C}$. The measurements over different pulses are supposed to be independent, which means

$$\operatorname{vec}(\mathbf{Y}) \sim \mathbb{C}\mathcal{N}_{NM}\left(\operatorname{vec}(\mathbf{W}\mathbf{X}\mathbf{\Phi}(\mathbf{v})), \mathbf{C} \otimes \mathbf{I}_M\right), \tag{27}$$

where $\otimes$ denotes Kronecker product. Accordingly, the OFDM measurements are distributed as

$$\mathbf{Y} \sim \mathbb{C}\mathcal{N}_{N,M}\left(\mathbf{W}\mathbf{X}\mathbf{\Phi}(\mathbf{v}), \mathbf{C} \otimes \mathbf{I}_M\right). \tag{28}$$

4. Detection Test

In low grazing angle scenario, received signals are the sum of signals along different paths, which form the complicated measurements. The essence of detection is to judge whether a target is present or not in the range cell under test. This is a classical two-hypothesis detection problem. Therefore, we construct a decision problem to choose between two possible hypotheses: the null hypothesis (target-free hypothesis) and the alternate hypothesis (target-present hypothesis), which can be expressed as

$$\begin{aligned} &\mathscr{H}_0\text{: } \mathbf{X} = \mathbf{0}, \quad \mathbf{C} \text{ unknown}, \\ &\mathscr{H}_1\text{: } \mathbf{X} \neq \mathbf{0}, \quad \mathbf{v}, \mathbf{C} \text{ unknown}. \end{aligned} \tag{29}$$

The measurements $\mathbf{Y}$ in two hypotheses are distributed as

$$\mathbf{Y} \sim \begin{cases} \mathscr{H}_0\text{: } \mathbb{C}\mathcal{N}_{N,M}\left(\mathbf{0}, \mathbf{C} \otimes \mathbf{I}_M\right), & \mathbf{C} \text{ unknown}, \\ \mathscr{H}_1\text{: } \mathbb{C}\mathcal{N}_{N,M}\left(\mathbf{W}\mathbf{X}\boldsymbol{\Phi}\left(\mathbf{v}\right), \mathbf{C} \otimes \mathbf{I}_M\right), & \mathbf{v}, \mathbf{C} \text{ unknown}. \end{cases} \tag{30}$$

According to the classical target detection theory, Neyman-Pearson (NP) detector is the optimal detector which maximizes the probability of detection at a constant probability of false alarm. However, the target velocity $\mathbf{v}$ and clutter covariance $\mathbf{C}$ are unknown, and GLRT detector is used instead where the unknown parameters are replaced with their maximum likelihood estimates (MLEs). The formulation of GLRT is [24]

$$\mathrm{GLR}\left(\mathbf{v}\right) = \frac{f\left(\mathbf{Y} \mid \mathscr{H}_1, \mathbf{v}, \widehat{\mathbf{X}}, \widehat{\mathbf{C}}_1\right)}{f\left(\mathbf{Y} \mid \mathscr{H}_0, \widehat{\mathbf{C}}_0\right)} \underset{\mathscr{H}_0}{\overset{\mathscr{H}_1}{\lessgtr}} \gamma, \tag{31}$$

where $f(\mathbf{Y} \mid \mathscr{H}_1)$ and $f(\mathbf{Y} \mid \mathscr{H}_0)$ are the likelihood functions under $\mathscr{H}_1$ and $\mathscr{H}_0$, respectively. γ is the threshold that the detector is compared with. $\widehat{\mathbf{X}}$ and $\widehat{\mathbf{C}}_1$ are the MLE of $\mathbf{X}$ and $\mathbf{C}$ under $\mathscr{H}_1$ while $\widehat{\mathbf{C}}_0$ is the MLE of $\mathbf{C}$ under $\mathscr{H}_0$.

Definition 1. If the random matrix $\mathbf{Y}(N \times M)$ is distributed as a matrix variate normal distribution (MVND) with mean $\mathbf{M}(N \times M)$ and covariance $\boldsymbol{\Omega} \otimes \boldsymbol{\Sigma}$, we use the notation $\mathbf{Y} \sim \mathbb{C}\mathcal{N}_{N,M}(\mathbf{M}, \boldsymbol{\Omega} \otimes \boldsymbol{\Sigma})$ and the probability density function (PDF) is given by [25]

$$f\left(\mathbf{Y}\right) = \frac{\exp\left(-\left(1/2\right)\mathrm{tr}\left[\boldsymbol{\Omega}^{-1}\left(\mathbf{Y}-\mathbf{M}\right)\boldsymbol{\Sigma}^{-1}\left(\mathbf{Y}-\mathbf{M}\right)^H\right]\right)}{\left(2\pi\right)^{NM/2}\left|\boldsymbol{\Omega}\right|^{N/2}\left|\boldsymbol{\Sigma}\right|^{M/2}}, \tag{32}$$

where $\mathrm{tr}(\cdot)$ is the trace of matrix. $\boldsymbol{\Omega}$ and $\boldsymbol{\Sigma}$ are positive definite covariance matrices over the column and row of $\mathbf{Y}$. $\boldsymbol{\Omega}$ is an $N \times N$ matrix and $\boldsymbol{\Sigma}$ is an $M \times M$ matrix which are defined as [25]

$$\begin{aligned} \boldsymbol{\Omega} &= E\left[\left(\mathbf{Y}-\mathbf{M}\right)\left(\mathbf{Y}-\mathbf{M}\right)^H\right], \\ \boldsymbol{\Sigma} &= E\left[\left(\mathbf{Y}-\mathbf{M}\right)^H\left(\mathbf{Y}-\mathbf{M}\right)\right]. \end{aligned} \tag{33}$$

According to the above descriptions, we can derive PDFs of the measurements under two hypotheses:

$$f\left(\mathbf{Y} \mid \mathscr{H}_0\right) = \frac{\exp\left(-\left(1/2\right)\mathrm{tr}\left[\mathbf{C}_0^{-1}\mathbf{Y}\mathbf{Y}^H\right]\right)}{\left(2\pi\right)^{NM/2}\left|\mathbf{C}_0\right|^{N/2}}, \tag{34}$$

$$f\left(\mathbf{Y} \mid \mathscr{H}_1\right) = \frac{\exp\left(-\left(1/2\right)\mathrm{tr}\left[\mathbf{C}_1^{-1}\left(\mathbf{Y}-\mathbf{W}\mathbf{X}\boldsymbol{\Phi}\left(\mathbf{v}\right)\right)\left(\mathbf{Y}-\mathbf{W}\mathbf{X}\boldsymbol{\Phi}\left(\mathbf{v}\right)\right)^H\right]\right)}{\left(2\pi\right)^{NM/2}\left|\mathbf{C}_1\right|^{N/2}}. \tag{35}$$

The log-likelihood function of (35) is

$$\begin{aligned} \ln f\left(\mathbf{Y} \mid \mathscr{H}_1\right) &= -\frac{MN}{2}\ln\left(2\pi\right) - \frac{N}{2}\ln\left|\mathbf{C}_1\right| \\ &\quad - \frac{1}{2}\mathrm{tr}\left[\mathbf{C}_1^{-1}\left(\mathbf{Y}-\mathbf{W}\mathbf{X}\boldsymbol{\Phi}\left(\mathbf{v}\right)\right)\left(\mathbf{Y}-\mathbf{W}\mathbf{X}\boldsymbol{\Phi}\left(\mathbf{v}\right)\right)^H\right]. \end{aligned} \tag{36}$$

Taking derivative of (36) with respect to $\mathbf{C}_1$ and making it equal to zero, the MLE of $\mathbf{C}_1$ is

$$\widehat{\mathbf{C}}_1 = \frac{1}{N}\left(\mathbf{Y}-\mathbf{W}\mathbf{X}\boldsymbol{\Phi}\left(\mathbf{v}\right)\right)\left(\mathbf{Y}-\mathbf{W}\mathbf{X}\boldsymbol{\Phi}\left(\mathbf{v}\right)\right)^H. \tag{37}$$

Substituting (37) into (36) yields

$$\widehat{\mathbf{X}}_{\mathrm{ML}} = \arg\min_{\mathbf{X}} \ln\left|\left(\mathbf{Y}-\mathbf{W}\mathbf{X}\boldsymbol{\Phi}\left(\mathbf{v}\right)\right)\left(\mathbf{Y}-\mathbf{W}\mathbf{X}\boldsymbol{\Phi}\left(\mathbf{v}\right)\right)^H\right|. \tag{38}$$

Usually, the scattering matrix $\widehat{\mathbf{X}}$ does not yield a close-form MLE expression. However, noting that $\mathbf{X}$ has a block-diagonal structure, it turns out to be a block-diagonal growth curve (BDGC) problem. Reference [26] derived the approximate maximum likelihood (AML) estimator for $\mathbf{X}$ which is given by

$$\hat{\mathbf{x}}_{\mathrm{AML}} = \mathrm{vecb}\left(\widehat{\mathbf{X}}\right) = \left(\boldsymbol{\Gamma}^H\boldsymbol{\Gamma}\right)^{-1}\boldsymbol{\Gamma}^H\mathrm{vec}\left(\mathbf{T}^{-1/2}\mathbf{X}\boldsymbol{\Pi}_{\Phi}\right), \tag{39}$$

where

$$\begin{aligned} \boldsymbol{\Gamma} &\triangleq \boldsymbol{\Phi}^T \circledast \left(\mathbf{T}^{1/2}\mathbf{W}\right), \\ \mathbf{T} &\triangleq \mathbf{Y}\boldsymbol{\Pi}_{\Phi}^{\perp}\mathbf{Y}^H, \\ \boldsymbol{\Pi}_{\Phi} &\triangleq \boldsymbol{\Phi}\left(\mathbf{v}\right)^H\left(\boldsymbol{\Phi}\left(\mathbf{v}\right)\boldsymbol{\Phi}\left(\mathbf{v}\right)^H\right)^{-}\boldsymbol{\Phi}\left(\mathbf{v}\right), \\ \boldsymbol{\Pi}_{\Phi}^{\perp} &\triangleq \mathbf{I} - \boldsymbol{\Pi}_{\Phi}, \end{aligned} \tag{40}$$

$\mathrm{vecb}(\cdot)$ and $\circledast$ denote block-diagonal matrix vectorization operator and generalized Khatri-Rao product [27], respectively, $\boldsymbol{\Pi}_{\Phi}$ and $\boldsymbol{\Pi}_{\Phi}^{\perp}$ are orthogonal projection matrix of $\boldsymbol{\Phi}(\mathbf{v})$, and $(\cdot)^{-}$ represents generalized inverse of matrix (e.g., a generalized inverse of matrix $\mathbf{S}$ is defined as $\mathbf{S}^{-}$ such that $\mathbf{S}\mathbf{S}^{-}\mathbf{S} = \mathbf{S}$) [27].

The log-likelihood function of (34) is

$$\ln f\left(\mathbf{Y} \mid \mathscr{H}_0\right) = -\frac{MN}{2}\ln\left(2\pi\right) - \frac{N}{2}\ln\left|\mathbf{C}_0\right| - \frac{1}{2}\mathrm{tr}\left[\mathbf{C}_0^{-1}\mathbf{Y}\mathbf{Y}^H\right]. \tag{41}$$

Taking derivative of (41) with respect to $\mathbf{C}_0$ and making it equal to zero, we get MLE of $\mathbf{C}_0$:

$$\widehat{\mathbf{C}}_0 = \frac{1}{N}\mathbf{Y}\mathbf{Y}^H. \tag{42}$$

Substituting (34), (35), (37), and (42) into (31), the GLRT detector is

$$\begin{aligned}\mathrm{GLR}(\mathbf{v}) &= \frac{\left|\widehat{\mathbf{C}}_0\right|}{\left|\widehat{\mathbf{C}}_1\right|} \\ &= \frac{\left|(1/N)\,\mathbf{Y}\mathbf{Y}^H\right|}{\left|(1/N)\left(\mathbf{Y}-\mathbf{W}\widehat{\mathbf{X}}\boldsymbol{\Phi}(\mathbf{v})\right)\left(\mathbf{Y}-\mathbf{W}\widehat{\mathbf{X}}\boldsymbol{\Phi}(\mathbf{v})\right)^H\right|}.\end{aligned} \tag{43}$$

Since target velocity $\mathbf{v}$ is unknown, it can be estimated through $\hat{\mathbf{v}} = \arg\max_{\mathbf{v}} \mathrm{GLR}(\mathbf{v})$ and the GLRT detector becomes

$$\max_{\mathbf{v}} \mathrm{GLR}(\mathbf{v}) = \mathrm{GLR}(\hat{\mathbf{v}}) \underset{\mathscr{H}_0}{\overset{\mathscr{H}_1}{\lessgtr}} \gamma. \tag{44}$$

5. Adaptive Waveform Design

In this section, we develop an adaptive waveform design method based on maximizing the Mahalanobis-distance to improve the detection performance. Since the target scattering coefficients vary with different subcarriers, we may change the transmitted weights $\mathbf{W}$ accordingly. From (30) we know that the measurement $\mathbf{Y}$ is distributed as $\mathbb{C}\mathcal{N}_{N,M}(\mathbf{W}\mathbf{X}\boldsymbol{\Phi}(\mathbf{v}), \mathbf{C}\otimes\mathbf{I}_M)$ under $\mathscr{H}_1$ hypothesis and $\mathbb{C}\mathcal{N}_{N,M}(0, \mathbf{C}\otimes\mathbf{I}_M)$ under $\mathscr{H}_0$ hypothesis. The squared Mahalanobis-distance is used to distinguish the above two distributions. It is noticeable that the column of $\mathbf{Y}$ is uncorrelated, which means that the measurements between different pulses are independent. The sum of squared Mahalanobis-distance over different pulses is given by [28]

$$d^2 = \sum_{m=0}^{M-1} \beta_m \left(\mathbf{W}\mathbf{X}\boldsymbol{\Phi}(:,m)\right)^H \mathbf{C}^{-1}\left(\mathbf{W}\mathbf{X}\boldsymbol{\Phi}(:,m)\right), \tag{45}$$

where β_m is a positive number and denotes the weight of Mahalanobis-distance over the mth pulse, satisfying $\sum_{m=0}^{M-1}\beta_m = 1$. To maximize the detection performance, we can formulate the optimization as

$$\begin{aligned}\mathbf{w}_{\mathrm{opt}} = \arg\max_{\mathbf{W}\in\mathbb{C}^N} \quad & \left[\sum_{m=0}^{M-1} \beta_m \left(\mathbf{W}\mathbf{X}\boldsymbol{\Phi}(:,m)\right)^H \mathbf{C}^{-1}\left(\mathbf{W}\mathbf{X}\boldsymbol{\Phi}(:,m)\right)\right], \\ \text{subject to} \quad & \mathbf{w}^H\mathbf{w} = 1.\end{aligned} \tag{46}$$

The scattering coefficients are constant from pulse to pulse and the measurement noise is uncorrelated between different pulses; thus β_m is a constant number; that is, $\beta_m = 1/M$ for $m = 0, 1, \ldots, M-1$. Since

$$\begin{aligned}&\left(\mathbf{W}\mathbf{X}\boldsymbol{\Phi}(:,m)\right)^H \mathbf{C}^{-1}\left(\mathbf{W}\mathbf{X}\boldsymbol{\Phi}(:,m)\right) \\ &\quad= \mathrm{tr}\left(\boldsymbol{\Phi}(:,m)^H\mathbf{X}^H\mathbf{W}^H\mathbf{C}^{-1}\mathbf{W}\mathbf{X}\boldsymbol{\Phi}(:,m)\right) \\ &\quad= \mathrm{tr}\left(\mathbf{C}^{-1}\mathbf{W}\mathbf{X}\boldsymbol{\Phi}(:,m)\,\boldsymbol{\Phi}(:,m)^H\mathbf{X}^H\mathbf{W}^H\right),\end{aligned} \tag{47}$$

the following theorem [11] is used to simplify the above equation:

$$\mathrm{tr}\left(\mathbf{S}_1\mathbf{A}\mathbf{S}_2\mathbf{A}^H\right) = \mathbf{a}^H\left[\mathbf{S}_2^T\odot\mathbf{S}_1\right]\mathbf{a}, \tag{48}$$

where $\mathbf{a}\in\mathbb{C}^N$ and $\mathbf{A} = \mathrm{diag}(\mathbf{a})$. $\odot$ denotes element-wise Hadamard product. Combining (47) and (48), we get

$$\begin{aligned}\mathbf{w}_{\mathrm{opt}} = \arg\max_{\mathbf{W}\in\mathbb{C}^N} \quad & \left(\frac{1}{M}\right)\mathbf{w}^H\left[\sum_{m=0}^{M-1}\left(\mathbf{X}\boldsymbol{\Phi}(:,m)\,\boldsymbol{\Phi}(:,m)^H\mathbf{X}^H\right)^T\odot\mathbf{C}^{-1}\right]\mathbf{w}, \\ \text{subject to} \quad & \mathbf{w}^H\mathbf{w} = 1.\end{aligned} \tag{49}$$

From (49) we know that the optimization problem is reduced to eigenvalue eigenvector problem and $\mathbf{w}_{\mathrm{opt}}$ is the eigenvector corresponding to the largest eigenvalue of $[\sum_{m=0}^{M-1}(\mathbf{X}\boldsymbol{\Phi}(:,m)\boldsymbol{\Phi}(:,m)^H\mathbf{X}^H)^T\odot\mathbf{C}^{-1}]$.

6. Numerical Results

In this section, several numerical examples are presented to illustrate the performance of proposed detector. For simplicity, we consider 2D scenario as shown in Figure 2. The simulation parameters are shown in Table 1.

We use Monte Carlo simulations to realize the following results for the analytical expression between false alarm rate and threshold cannot be acquired. The relation between probability of false alarm rate and detection threshold corresponding to different carrier numbers is shown in Figure 3. The curves show that when false alarm rate is kept fixed,

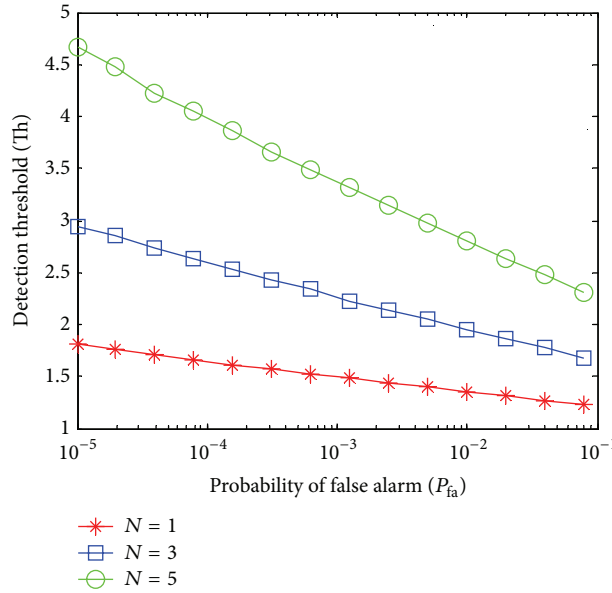

Figure 3: Detection threshold versus probability of false alarm at different carrier numbers.

Table 1: Parameter settings of the simulations.

Parameters	Values
Height of target	200 m
Velocity of target	$[141.4 \quad 141.4]^T$ m/s
Scattering coefficient matrix of target $\mathbf{X}$	$\mathbb{C}\mathcal{N}(0, 1)$
Height of radar platform	100 m
Velocity of radar platform	$[0 \quad 0]^T$ m/s
Relative distance between radar and target	5 km
Multipath number P	3
Carrier frequency f_0	1 GHz
Bandwidth B	100 MHz
Carrier numbers N	3
Frequency weights $\mathbf{W}$	$1/\sqrt{N}\mathbf{I}_N$
Pulse number M	30
Pulse repetition interval T_r	2 ms

the higher the subcarrier number, the higher the threshold. Signal-to-noise ratio (SNR) is defined as [11]

$$\text{SNR} = \frac{(1/N)\sum_{m=1}^{M}\left(\mathbf{W}\mathbf{X}\boldsymbol{\phi}(m,\mathbf{v})\right)^H \mathbf{W}\mathbf{X}\boldsymbol{\phi}(m,\mathbf{v})}{\text{tr}(\mathbf{C})}. \quad (50)$$

The effect of multipath number on the detection performance is shown in Figure 4, where the path number is set as $P = 1$ and $P = 3$. Figures 4(a) and 4(b) show P_d versus SNR with different P_{fa}s and P_d versus P_{fa} when SNR is fixed to −20 dB, respectively. The curves show that the detection performance is improved with the increasing of multipath number. Consequently, the derived detector with OFDM waveform could exploit multipath reflections to enhance the detection performance.

In Figure 5, we analyze the effect of subcarrier number on the performance of proposed detector, where the subcarrier number is set as $N = 1$, 3, and 5, respectively. Figures 5(a) and 5(b) show P_d versus SNR when $P_{\text{fa}} = 10^{-3}$ and P_d versus P_{fa} when SNR is fixed to −20 dB, respectively. The detection performance is improved with the increasing of subcarrier number. The results demonstrate that the detection performance is improved due to the frequency diversity in an OFDM radar system.

Figure 6 shows that the detection performance varies with the target height, which is set as 200 m, 400 m, and 600 m, respectively. Figure 6(a) shows P_d versus SNR when $P_{\text{fa}} = 10^{-3}$ while Figure 6(b) shows P_d versus P_{fa} when SNR is fixed to −20 dB. The results demonstrate that detection performance decreases with the increasing of target height in low grazing angle scenario. This can be explained that as the target height increases, the grazing angle gets larger and the complex reflection coefficient over indirect paths becomes smaller which is shown in Figure 7. Thus, the detection performance deteriorates.

In Figure 8, we analyze the effect of varying the directions of target velocity vector on the detection performance. Here, $\mathbf{v}^T = [100 \quad 0]$, $[71.7 \quad 71.7]$, and $[0 \quad 100]$ m/s, respectively. Figures 8(a) and 8(b) show P_d versus SNR when $P_{\text{fa}} = 10^{-3}$ and P_d versus P_{fa} when SNR is fixed to −20 dB, respectively. In this paper, we take advantage of multipath propagation by exploiting multiple Doppler shifts corresponding to the projections of target velocity on each of the multipath components. When the angle between the target velocity vector and radar LOS decreases, the Doppler frequency of

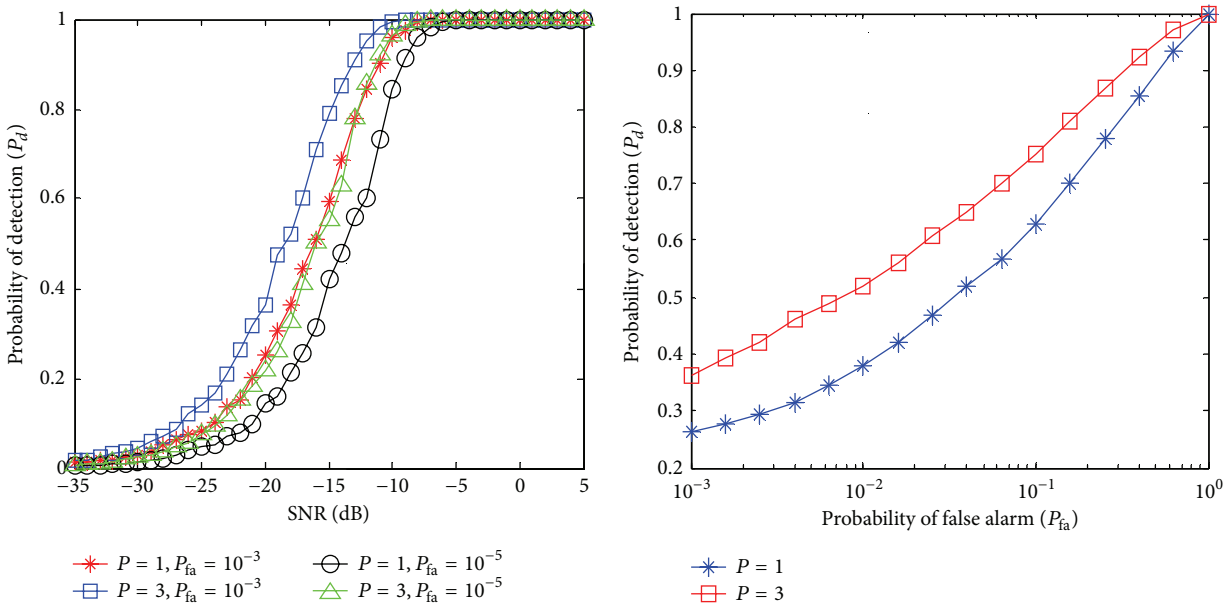

(a) P_d versus SNR with different P_{fa}s

(b) P_d versus P_{fa} when SNR = −20 dB

Figure 4: Effect of the path number on the detection performance.

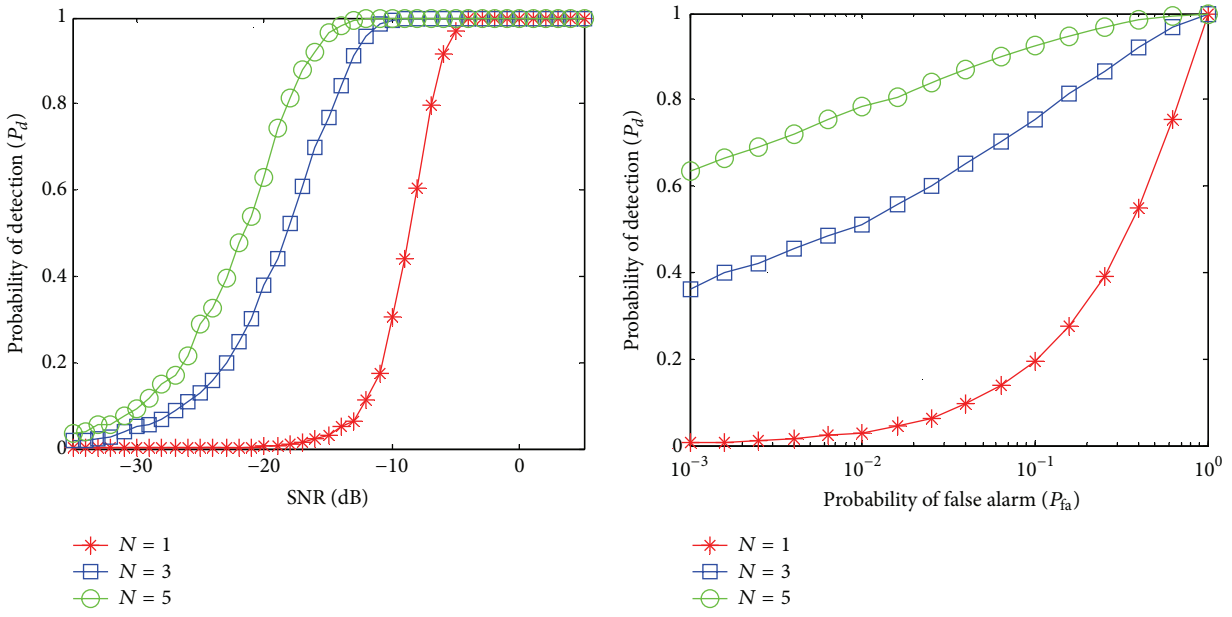

(a) P_d versus SNR when $P_{fa} = 10^{-3}$

(b) P_d versus P_{fa} when SNR = −20 dB

Figure 5: Effect of the subcarrier number on the detection performance.

received signal will increase. Thus the detection performance is improved.

In Figure 9, we show the detection performance improvement due to the adaptive waveform design. Figure 9(a) shows P_d versus SNR when $P_{fa} = 10^{-3}$ while Figure 9(b) shows P_d versus P_{fa} when SNR is fixed to −20 dB. We assume that the transmitted waveform in the first M pulses has equal weights; that is, $\mathbf{w} = 1/\sqrt{N}\mathbf{I}$. Then, based on (49), we compute $\mathbf{w}_{opt}$ for the next M pulses. As is shown, compared with fixed waveform, the detection performance is improved due to the adaptive waveform method proposed in this paper.

Finally, to validate our method in non-Gaussian scenarios, we conduct additional experiments using compound K-distribution, whose PDF is [29]

$$f(z) = \frac{\sqrt{2\nu/\mu}}{\Gamma(\nu)} \left(\sqrt{\frac{2\nu}{\mu}} z\right)^{\nu} K_{\nu-1}\left(\sqrt{\frac{2\nu}{\mu}} z\right) \quad (51)$$

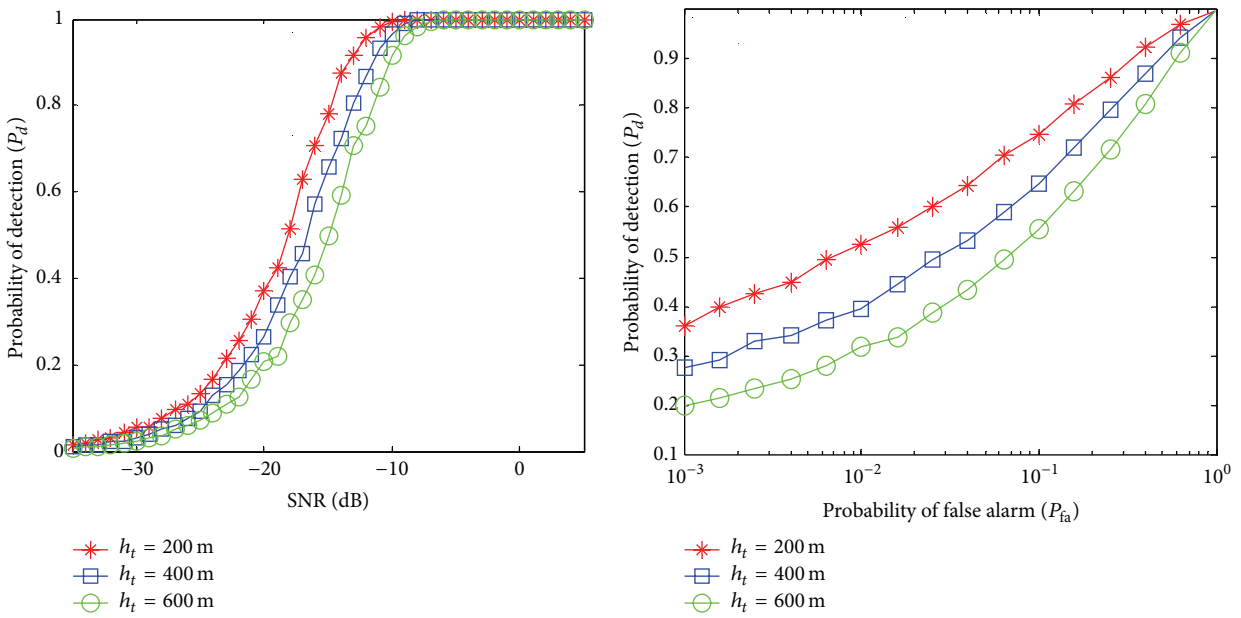

(a) P_d versus SNR when $P_{fa} = 10^{-3}$

(b) P_d versus P_{fa} when SNR = −20 dB

Figure 6: Detection performance varies with target height.

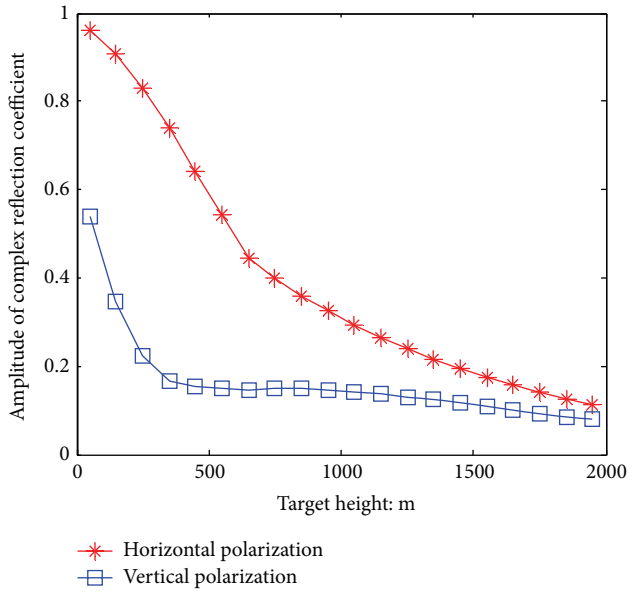

Figure 7: Amplitude of complex reflection coefficient varies with target height.

and the texture follows a gamma distribution with PDF

$$f(u) = \frac{1}{\Gamma(\nu)} \left(\frac{\nu}{\mu}\right)^{\nu} u^{\nu-1} e^{-\nu/\mu u} \kappa(u), \tag{52}$$

where $\Gamma(\cdot)$ is the Eulerian gamma function, $\kappa(\cdot)$ is the unit step function, and $K_{\nu-1}(\cdot)$ is the modified Bessel function of second kind with order $\nu - 1$. μ and ν are the scale and shape parameter, respectively. The speckle component is assumed to be a Gaussian distribution with exponential correlation structure covariance matrix [30]:

$$[\mathbf{C}]_{i,j} = \rho^{|i-j|}, \quad \text{for } i, j = 0, 1, \ldots, N-1, \tag{53}$$

where ρ is one-lag correlation coefficient. The other parameters are the same as in Table 1.

Figure 10 shows the detection performance with different path numbers ($P = 1, 3$) in Gaussian and compound

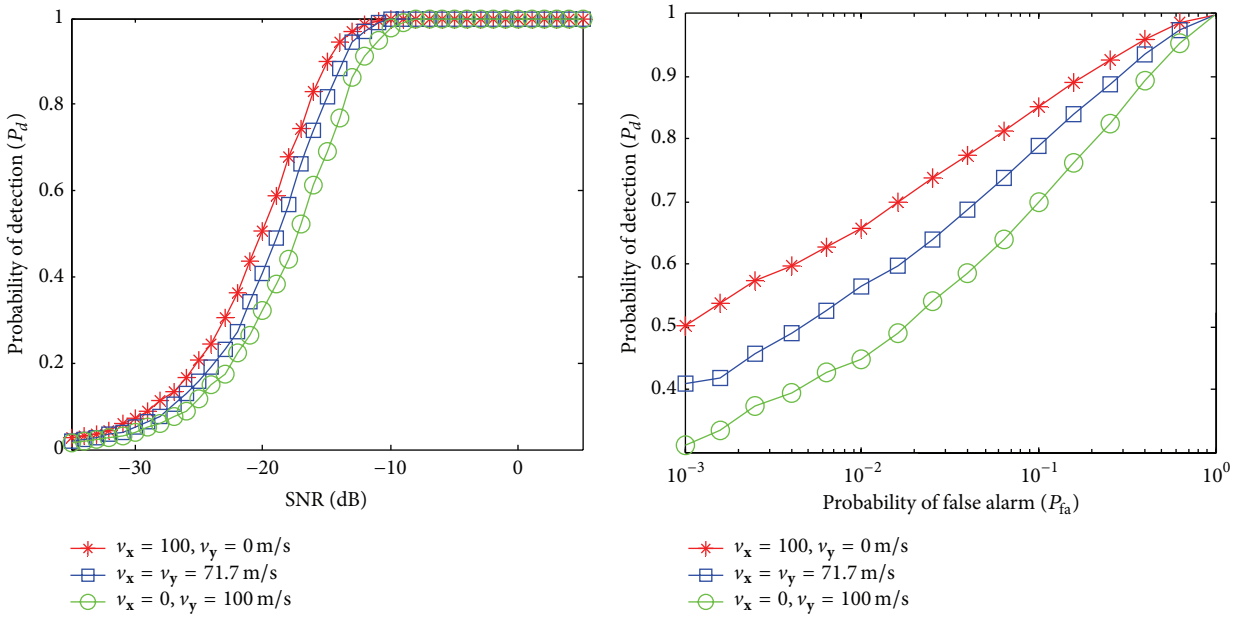

(a) P_d versus SNR when $P_{fa} = 10^{-3}$

(b) P_d versus P_{fa} when SNR = −20 dB

Figure 8: Effect of different directions of target velocity on detection performance.

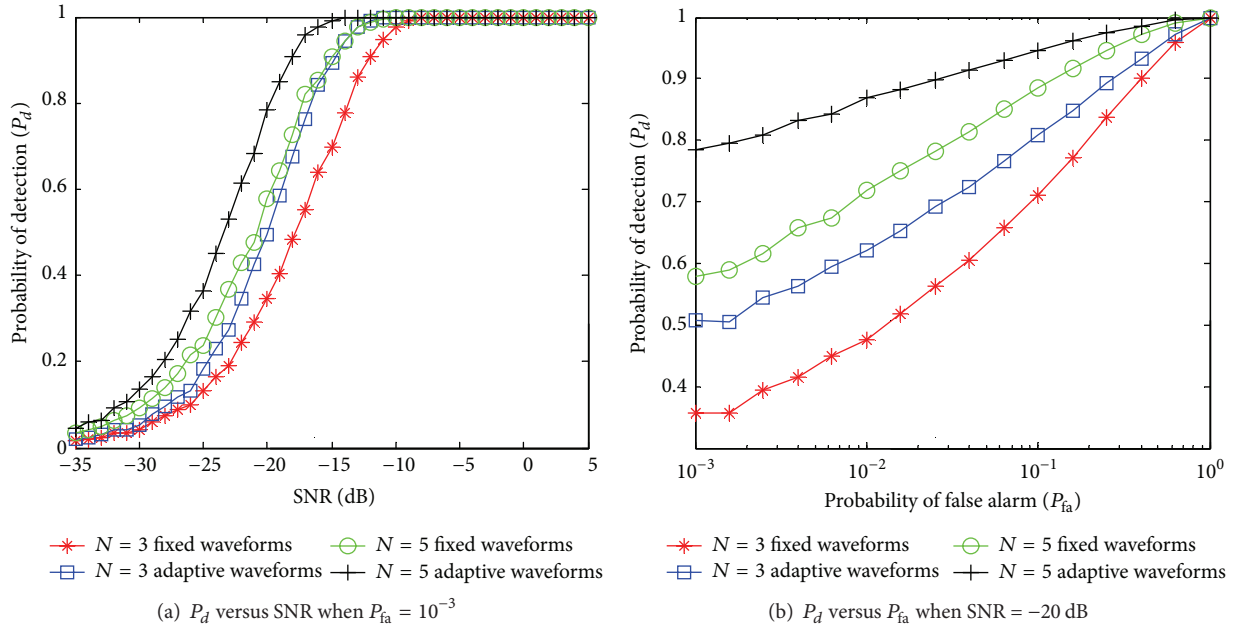

(a) P_d versus SNR when $P_{fa} = 10^{-3}$

(b) P_d versus P_{fa} when SNR = −20 dB

Figure 9: Comparison of detection performance with fixed waveform and adaptive waveform.

K-distribution clutter and Figure 11 shows the detection performance with fixed and adaptive waveform design in Gaussian and compound K-distribution clutter. We find that, in compound K-distribution, the detector derived under Gaussian assumption also yields improved performance by taking advantage of multipath effect and adaptive waveform design of OFDM radar. However, the performance gap exists due to the model mismatch.

7. Conclusions

In this paper, we address the problem of target detection in low grazing angle scenario with OFDM radar. We consider the realistic physical and statistical effects to make the propagation model more realistic. Based on the characteristics of OFDM signal, we develop a GLRT detector and show that detection performance is improved due to the multipath utilization and frequency diversity of OFDM

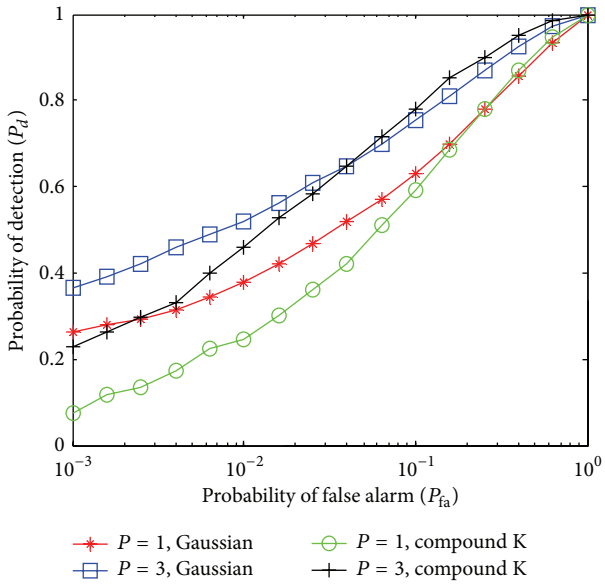

FIGURE 10: Effect of the multipath number on detection performance in Gaussian and compound K-distribution clutter.

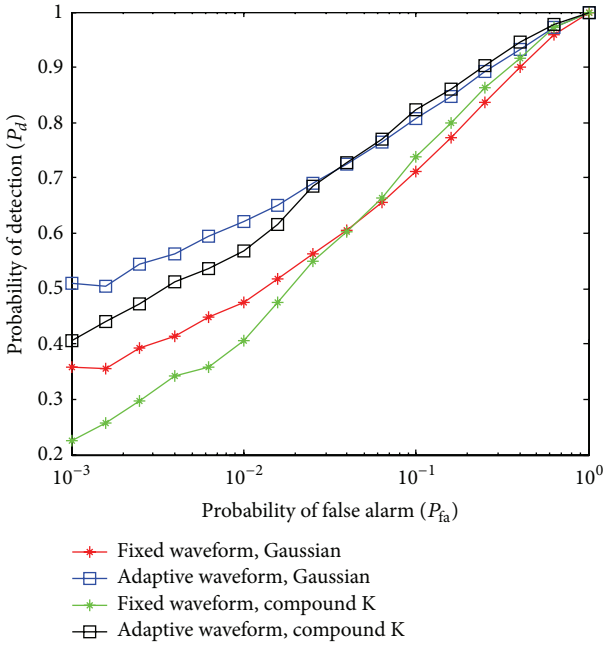

FIGURE 11: Comparison of detection performance with fixed and adaptive waveform in Gaussian and compound K-distribution clutter (P = 3).

radar. Then an adaptive waveform design method based on Mahalanobis-distance is proposed and the detection performance is improved due to the optimized transmitted frequency weights. Finally, we show that the GLRT detector derived under Gaussian assumption yields improved performance in compound K-distribution clutter due to the multipath utilization and adaptive waveform design. However, the performance gap exists and we will extend our work to more general situations in the future work.

Conflict of Interests

The authors declare that there is no conflict of interests regarding the publication of this paper.

Acknowledgment

This work was supported in part by the National Science Foundation of China under Grant no. 61401475.

References

[1] D. K. Barton, "Low-angle radar tracking," *Proceedings of the IEEE*, vol. 62, no. 6, pp. 687–704, 1974.

[2] S. L. Silon and B. D. Carlson, "Radar detection in multipath," *IEE Proceedings—Radar, Sonar and Navigation*, vol. 146, no. 1, pp. 45–54, 1999.

[3] J.-H. Zhao and J.-Y. Yang, "Frequency diversity to low-angle detecting using a highly deterministic multipath signal model," in *Proceedings of the 6th CIE International Conference on Radar (ICR '06)*, pp. 1–5, IEEE, Shanghai, China, October 2006.

[4] M. Jankiraman, B. J. Wessels, and P. van Genderen, "Design of a multifrequency FMCW radar," in *Proceedings of the 28th European Microwave Conference (EuMC '98)*, pp. 584–589, Amsterdam, The Netherlands, October 1998.

[5] N. Levanon, "Multifrequency complementary phase-coded radar signal," *IEE Proceedings: Radar, Sonar and Navigation*, vol. 147, no. 6, pp. 276–284, 2000.

[6] R. Mohseni, A. Sheikhi, and M. A. Masnadi-Shirazi, "Multicarrier constant envelope OFDM signal design for radar applications," *AEU: International Journal of Electronics and Communications*, vol. 64, no. 11, pp. 999–1008, 2010.

[7] G. Lellouch, A. Mishra, and M. Inggs, "Impact of the Doppler modulation on the range and Doppler processing in OFDM radar," in *Proceedings of the IEEE Radar Conference (RadarCon '14)*, pp. 803–808, Cincinnati, Ohio, USA, May 2014.

[8] S. Sen and A. Nehorai, "Adaptive design of OFDM radar signal with improved wideband ambiguity function," *IEEE Transactions on Signal Processing*, vol. 58, no. 2, pp. 928–933, 2010.

[9] G. Lellouch and A. K. Mishra, "Optimization of OFDM radar waveforms using geneticalgorithms," http://arxiv.org/abs/1405.4894.

[10] K. Huo, Z. K. Qiu, Y. X. Liu, and W. D. Jiang, "An adaptive waveform design method for OFDM cognitive radar," in *Proceedings of the International Radar Conference*, pp. 1–5, IEEE, Lille, France, October 2014.

[11] S. Sen and A. Nehorai, "Adaptive OFDM radar for target detection in multipath scenarios," *IEEE Transactions on Signal Processing*, vol. 59, no. 1, pp. 78–90, 2011.

[12] S. Sen, M. Hurtado, and A. Nehorai, "Adaptive OFDM radar for detecting a moving target in urban scenarios," in *Proceedings of the International Waveform Diversity and Design Conference (WDD '09)*, pp. 268–272, IEEE, Orlando, Fla, USA, February 2009.

[13] S. Sen, G. Tang, and A. Nehorai, "Multiobjective optimization of OFDM radar waveform for target detection," *IEEE Transactions on Signal Processing*, vol. 59, no. 2, pp. 639–652, 2011.

[14] S. Sen, G. Tang, and A. Nehorai, "OFDM radar waveform design for sparsity-based multi-target tracking," in *Proceedings of the*

International Waveform Diversity and Design Conference (WDD '10), pp. 18–22, IEEE, Niagara Falls, Canada, August 2010.

[15] S. Kafshgari and R. Mohseni, "Fluctuating target detection in presence of non Gaussian clutter in OFDM radars," *AEU: International Journal of Electronics and Communications*, vol. 67, no. 10, pp. 885–893, 2013.

[16] W. D. White, "Low-angle radar tracking in the presence of multipath," *IEEE Transactions on Aerospace and Electronic Systems*, vol. 10, no. 6, pp. 835–852, 1974.

[17] S. Sen and A. Nehorai, "OFDM MIMO radar with mutual-information waveform design for low-grazing angle tracking," *IEEE Transactions on Signal Processing*, vol. 58, no. 6, pp. 3152–3162, 2010.

[18] H. V. Hitney, J. H. Richter, R. A. Pappert, K. D. Anderson, and G. B. Baumgartner Jr., "Tropospheric radio propagation assessment," *Proceedings of the IEEE*, vol. 73, no. 2, pp. 265–283, 1985.

[19] H. Hitney and R. Vieth, "Statistical assessment of evaporation duct propagation," *IEEE Transactions on Antennas and Propagation*, vol. 38, no. 6, pp. 794–799, 1990.

[20] M. W. Long, *Radar Reflectivity of Land Sea*, Artech House, 3rd edition, 2001.

[21] T. Lo and J. Litva, "Use of a highly deterministic multipath signal model in low-angle tracking," *IEE Proceedings F—Radar and Signal Processing*, vol. 138, no. 2, pp. 163–171, 1991.

[22] F. Gini, M. V. Greco, M. Diani, and L. Verrazzani, "Performance analysis of two adaptive radar detectors against non-Gaussian real sea clutter data," *IEEE Transactions on Aerospace and Electronic Systems*, vol. 36, no. 4, pp. 1429–1439, 2000.

[23] K. James Sangston, F. Gini, M. V. Greco, and A. Farina, "Structures for radar detection in compound gaussian clutter," *IEEE Transactions on Aerospace and Electronic Systems*, vol. 35, no. 2, pp. 445–458, 1999.

[24] S. M. Kay, *Fundamentals of Statistical Signal Processing: Detection Theory*, Prentice Hall PTR, Upper Saddle River, NJ, USA, 1998.

[25] T. W. Anderson, *An Introduction to Multivariate Statistical Analysis*, Wiley Series in Probability and Statistics, Wiley-Interscience, John Wiley & Sons, Hoboken, NJ, USA, 3rd edition, 2003.

[26] L. Xu, P. Stoica, and J. Li, "A block-diagonal growth curve model," *Digital Signal Processing*, vol. 16, no. 6, pp. 902–912, 2006.

[27] A. Dogandžić and A. Nehorai, "Generalized multivariate analysis of variance: a unified framework for signal processing in correlated noise," *IEEE Signal Processing Magazine*, vol. 20, no. 5, pp. 39–54, 2003.

[28] R. De Maesschalck, D. Jouan-Rimbaud, and D. L. Massart, "The Mahalanobis distance," *Chemometrics and Intelligent Laboratory Systems*, vol. 50, no. 1, pp. 1–18, 2000.

[29] E. Conte, M. Longo, and M. Lops, "Modelling and simulation of non-Rayleigh radar clutter," *IEE Proceedings F: Radar and Signal Processing*, vol. 138, no. 2, pp. 121–130, 1991.

[30] G. Cui, L. Kong, and X. Yang, "Multiple-input multiple-output radar detectors design in non-Gaussian clutter," *IET Radar, Sonar & Navigation*, vol. 4, no. 5, pp. 724–732, 2010.